J. Fluid Mech. (1999), *vol.* 379, *pp.* 279–302. Printed in the United Kingdom

Marangoni effects on the motion of an expanding or contracting bubble pinned at a submerged tube tip

By HARRIS WONG[1], DAVID RUMSCHITZKI[2] AND CHARLES MALDARELLI[2]

[1]Mechanical Engineering Department, Louisiana State University, Baton Rouge, LA 70803-6413, USA

[2]The Levich Institute and Chemical Engineering Department, The City College of CUNY, New York, NY 10031, USA

(Received 2 July 1996 and in revised form 11 August 1998)

This work studies the motion of an expanding or contracting bubble pinned at a submerged tube tip and covered with an insoluble Volmer surfactant. The motion is driven by constant flow rate Q into or out of the tube tip. The purpose is to examine two central assumptions commonly made in the bubble and drop methods for measuring dynamic surface tension, those of uniform surfactant concentration and of purely radial flow. Asymptotic solutions are obtained in the limit of the capillary number $Ca \to 0$ with the Reynolds number $Re = o(Ca^{-1})$, non-zero Gibbs elasticity (G), and arbitrary Bond number (Bo). ($Ca = \mu Q/a^2\sigma_c$, where μ is the liquid viscosity, a is the tube radius, and σ_c is the clean surface tension.) This limit is relevant to dynamic-tension experiments, and gives $M \to \infty$, where $M = G/Ca$ is the Marangoni number. We find that in this limit the deforming bubble at each instant in time takes the static shape. The surfactant distribution is uniform, but its value varies with time as the bubble area changes. To maintain a uniform distribution at all times, a tangential flow is induced, the magnitude of which is more than twice that in the clean case. This is in contrast to the surface-immobilizing effect of surfactant on an isolated translating bubble. These conclusions are confirmed by a boundary integral solution of Stokes flow valid for arbitrary Ca, G and Bo. The uniformity in surfactant distribution validates the first assumption in the bubble and drop methods, but the enhanced tangential flow contradicts the second.

1. Introduction

Surfactant adsorption or desorption at an interface is usually studied by expanding or contracting the interfacial area and measuring the change in surface tension as a surfactant adsorbs onto or desorbs from the perturbed surface. An equation of state relates the tension to the surface surfactant concentration. Comparison with the predictions of transport models determines the kinetic rate constants and bulk diffusion coefficients (see the review by Chang & Franses 1995). Among the most useful methods for arranging the surfactant exchange are the expansion or contraction of bubbles or drops attached to a tube tip and with an adsorbed monolayer on their surfaces. The bubble or drop motion is slow so that the viscous and inertial forces exerted on the interface by the induced flow are much smaller than the surface tension forces. Thus, the capillary number $Ca \ll 1$, and the Weber number $We = Ca\,Re \ll 1$,

where Re is the Reynolds number. ($Ca = \mu Q/a^2\sigma_c$ and $Re = \rho Q/a\mu$, where a is the tube radius, σ_c is the clean surface tension, Q is the characteristic volume flow rate into or out of the tube tip, and μ and ρ are, respectively, the viscosity and density of the liquid.) For $Ca \ll 1$ and $Ca\,Re \ll 1$, the bubble or drop shape is governed by a static balance between the surface tension and gravitational forces, i.e. by the Young–Laplace equation.

In this paper, we study the fluid mechanics of a model system in which a pendant bubble, submerged in a liquid and attached to a tube tip, expands or contracts with an adsorbed, insoluble Volmer surfactant (Gaines 1966; Aveyard & Haydon 1973) on its surface for $Ca \ll 1$ and $Ca\,Re \ll 1$. Our purpose is to use the model results to examine the validity of two central assumptions commonly made in the bubble or drop techniques for measuring dynamic surface tension. We begin with a brief description of the bubble and drop techniques (§ 1.1), which sets the background for the elucidation in § 1.2 of the central assumptions we will examine.

1.1. *Bubble or drop dynamic-surface-tension measurement techniques*

These techniques measure the tension from the Young–Laplace equation either by analysing the interfacial shape (the pendant bubble or drop shape analysis method), determining the bubble or drop pressure (growing drop, maximum bubble pressure, and pulsating bubble methods), or measuring the weight of detached drops (drop weight method).

The shape analysis method employs large bubbles or drops so that gravity elongates the shape into a pendant form rather than a section of a sphere (see, for example, Miller, Joos & Fainerman 1994; Faour *et al.* 1996; Song & Springer 1996; der Rio & Neumann 1997). In practice, this means that the Bond number must be larger than 0.05 ($Bo = \rho g a^2/\sigma_c$, where g is the acceleration due to gravity). A bubble or drop is first formed at the tip of a tube with the tip either facing up (bubble) or down (drop). After formation, surfactant molecules in the solution begin to adsorb onto the interface until the surface concentration reaches equilibrium. The interface is then contracted or expanded by changing the volume of the bubble or drop, causing the surfactant to exchange between the liquid and the interface. A video camera captures a silhouette of the bubble or drop, and the edge location is discretized and stored. Matching the instantaneous shapes to solutions of the Young–Laplace equation yields the tension as a function of time.

The growing drop method forms a hemispherical drop of surfactant solution in air at a tube tip, and then expands it (Passerone *et al.* 1991; Macleod & Radke 1993; Nagarajan & Wasan 1993; Zhang, Harris & Basaran 1994; Liggieri, Ravera & Passerone 1995). Surfactant molecules diffuse towards and adsorb onto the expanding drop surface. The tube diameter is small so that the drop grows as a section of a sphere. The drop pressure $P(t)$ (relative to the atmospheric pressure) is measured and the radius of the drop $R(t)$ is calculated from the measured liquid flow rate. The tension follows from the simplified form of the Young–Laplace equation: $\sigma(t) = \frac{1}{2}R(t)\,P(t)$, as dictated by the spherical geometry. The maximum bubble pressure method grows bubbles continuously from a tube tip, and records the maximum pressure when the bubble is hemispherical (see, for example, Miller *et al.* 1994; Hallowell & Hirt 1994). The spherical form of the Young–Laplace equation again yields the tension at the time of maximum pressure. This is the tension when the bubble is hemispherical, which occurs at a particular surface age, with the age of a freshly created bubble taken as zero. At a higher gas flow rate, a bubble takes less time to grow to be hemispherical, and the surface is less aged at the moment of maximum pressure.

Thus, by using different gas flow rates, the surface tension is determined for different surface ages. The pulsating bubble technique oscillates the area of a pinned bubble that is small enough to be a section of a sphere and continuously measures the pressure in the bubble and the radius of curvature (Chang & Franses 1994*a*, *b*). The simplified Young–Laplace equation again gives the oscillating tension from the continuously measured gas pressure and radius.

In the drop weight method, pendant drops form and detach from a tube tip (see the review by Miller *et al.* 1994). At the slow flow rates for which inertial and viscous forces are negligible, a drop detaches quasi-statically when surface tension cannot support its weight. Thus, the detached weight determines the tension at the moment of detachment. As with the maximum bubble pressure method, varying the flow rate accesses the tensions at different surface ages.

1.2. *The central assumptions in the bubble or drop techniques*

All of the above bubble or drop methods for the measurement of dynamic tension make two central assumptions. First, as the bubble or drop expands or contracts, the surface concentration remains uniform along the surface. Secondly, the surfactant in the bulk liquid is convected only radially from the centre of the bubble or drop, i.e. the tangential transport is negligible. All surfactant transport modelling begins by assuming that the bubble or drop is a sphere (or a section of a sphere), with an initial uniform concentration C_0 in the liquid and either zero surface concentration or a non-zero concentration Γ_0 in equilibrium with C_0. The models take the flow in the liquid (either inside the drop or outside the bubble) as only normal to the surface ($u_r = 1/4\pi r^2$). Here u_r is the radial velocity (scaled by Q/a^2) and r is the distance (scaled by a) from the centre of the spherical bubble or drop. The convective and diffusive transport of the bulk surfactant having concentration $C(r, t)$ (scaled by C_0) is also radial:

$$\frac{\partial C}{\partial t} + u_r \frac{\partial C}{\partial r} = \frac{1}{Pe} \nabla_r^2 C, \tag{1.1}$$

where Pe is the Péclet number ($= Q/aD$, D being the bulk diffusivity), t is time (scaled by a^3/Q) and ∇_r^2 is the (non-dimensional) r component of the spherical Laplacian. The surface concentration Γ (scaled by Γ_0) is assumed to be uniform and is determined by the overall surfactant mass balance:

$$\frac{\mathrm{d}\Gamma}{\mathrm{d}t} + \frac{\Gamma}{A}\frac{\mathrm{d}A}{\mathrm{d}t} = \frac{1}{Pe}\frac{aC_0}{\Gamma_0}\left[\frac{\partial C}{\partial r}\right]_{r=R}, \tag{1.2}$$

where A is the bubble or drop area (non-dimensionalized by a^2), and the right-hand side of (1.2) is the diffusive flux at the surface. The boundary conditions for these equations either equate the diffusive flux to the kinetic rate or require adsorption equilibrium if the kinetics are fast, i.e. if the process is diffusion controlled (see, for example, Nagarajan & Wasan 1993; Chang & Franses 1994*b*). If the expansion or contraction takes place in a short time, then diffusion changes only the bulk concentration next to the bubble surface in a thin boundary layer of thickness $\delta(t) \ll a$. For this case the transport equation becomes

$$\frac{\partial C}{\partial t} - \frac{n}{A}\frac{\mathrm{d}A}{\mathrm{d}t}\frac{\partial C}{\partial n} = \frac{1}{Pe}\frac{\partial^2 C}{\partial n^2}, \tag{1.3}$$

where n is the non-dimensional distance normal to the surface. Small penetration depth solutions have been developed by Hirt *et al.* (1990), Macleod & Radke (1994), and Joos & van Uffelen (1995), among others.

The validity of the two assumptions has yet to be established. When a bubble or drop expands or contracts from its initial equilibrium state, the surface surfactant concentration changes by two mechanisms. First, the surface surfactant is convected by a tangential flow induced by the motion of the bubble or drop. Wong *et al.* (1998) numerically calculated the tangential flow induced by the expansion or contraction of a clean bubble for $0.01 \leqslant Ca \leqslant 100$ and without inertia ($Re \ll 1$, $Ca\,Re \ll 1$). During contraction, for example, they found that the surface flow is from the bubble apex towards the tube tip. Thus, during contraction, the convection mechanism will carry the surfactant towards the tube tip, and increase the surfactant concentration there. The second mechanism, however, tends to increase the surfactant concentration at the bubble apex. This mechanism is the local area expansion or compression, which changes the local surfactant concentration. This local area expansion or compression is proportional to the normal velocity multiplied by the mean curvature. Because the bubble is pinned at the tube tip, the normal velocity is zero there and is usually highest at the bubble apex. Consequently, the local area change is zero at the rim and highest near the apex. In contraction, for example, the compression of interface at the apex is greater than that near the tube tip, and thus the surfactant concentration is higher at the apex than at the tip. This gradient in surfactant concentration is opposite to that created by the convection mechanism. Scaling arguments cannot decide which mechanism will dominate because the two terms representing the two mechanisms are both order one in the surfactant transport equation. Thus, a numerical solution is necessary to reveal the dominant mechanism of surfactant transport.

In this paper, we study surfactant distribution and tangential velocity induced by the Marangoni traction by numerically solving a model problem. We choose the expansion and contraction of a pinned bubble in a liquid. The bubble initially is at rest, with an adsorbed surfactant of uniform concentration Γ_0 on its surface. We assume for the purposes of illustration that the surfactant is insoluble. We first construct a formal asymptotic expansion in the limit $Ca \to 0$ with the Gibbs elasticity $G \neq 0$ (which gives $M \to \infty$, where $M = G/Ca$ is the Marangoni number), and obtain leading-order solutions. We find that the solutions of bubble shape and surface velocities apply not only to bubbles, but also to drops. The results show that the surface surfactant concentration is uniform. This, therefore, confirms the validity of the first assumption made in the bubble and drop techniques. To verify our asymptotic solution and its conclusions, we calculate the surface concentration and velocities using a boundary integral numerical scheme valid for $Re \ll 1$, $Ca\,Re \ll 1$, and arbitrary Ca and G. We demonstrate that as $Ca \to 0$ (or $M \to \infty$) the surfactant distribution becomes more uniform, and the tangential flow is enhanced. Thus, the second assumption in the bubble and drop techniques is incorrect. The numerical results also show that the local area compression or expansion is the dominant mechanism for determining the surfactant concentration gradient.

The enhanced tangential flow shows that surfactants have very different effects on the motions of a growing pinned bubble and a translating isolated bubble. A detached bubble rising in a surfactant solution will see a tangential flow from the nose to the back. This flow will sweep the adsorbed surface surfactant towards the back to generate a gradient in surfactant concentration and, thus, in surface tension. This creates an opposing Marangoni force, which eventually reduces the tangential surface velocity to zero to yield no slip on the bubble surface (Sadhal & Johnson 1983). This zero velocity might have motivated the second assumption, in which the tangential flow is neglected. However, a pinned bubble expanding or contracting in a surfactant solution will see its tangential flow enhanced by the surfactant, owing to

the non-uniform surface area expansion or compression. This conclusion holds in the limit the Marangoni number $M \to \infty$, which in general is associated with forming a no-slip surface on an isolated translating bubble. Thus, 'no-slip' ($M \to \infty$) on the surface of a pinned, expanding or contracting bubble implies an enhanced tangential flow, in contrast to the case of an isolated translating bubble.

We begin in § 2 by formulating the complete problem of bubble expansion or contraction. In § 3, using this formulation, we derive the asymptotic equations for the surface tangential velocity in the limit $Ca \to 0$. Section 4 gives the details of the boundary integral numerical method valid for arbitrary Ca and zero inertia. Results of these boundary integral calculations and their comparisons with the asymptotic results as $Ca \to 0$ are in § 5. Extensions of the conclusions to bulk soluble surfactants are discussed in § 6, and the paper concludes with a summary in § 7.

2. Mathematical model

Figure 1 shows the physical situation. A static, axisymmetric bubble sits at the tip of a semi-infinite tube of radius a in an incompressible Newtonian liquid of viscosity μ and density ρ. An insoluble surfactant is deposited onto the bubble surface, and the bubble relaxes to an equilibrium shape with a uniform surfactant concentration Γ_0. At time $t = 0$, one either expands or contracts the bubble at a constant volume flow rate Q. The liquid flow so generated obeys the equations:

$$Re\,Ca\left[\frac{\partial \boldsymbol{u}}{\partial t} + \boldsymbol{u}\cdot\nabla\boldsymbol{u}\right] = \nabla\cdot\boldsymbol{T} = -\nabla p + Ca\nabla^2\boldsymbol{u} - Bo\,\boldsymbol{e}_z, \tag{2.1a}$$

$$\nabla\cdot\boldsymbol{u} = 0, \tag{2.1b}$$

where $\boldsymbol{T}$ is the stress, $\boldsymbol{u}$ is the velocity, p is the pressure relative to $p(r \to \infty,\ z = 0)$, ∇ is the gradient operator, and $\boldsymbol{e}_z$ is an upward-pointing unit vector. A cylindrical coordinate system $(r,\ z)$ is set at the tube tip (figure 1). The capillary number $Ca \equiv \mu Q/a^2\sigma_c$ and the Bond number $Bo \equiv \rho g a^2/\sigma_c$ measure, respectively, the relative importance of viscous and gravity forces to capillary forces. In these dimensionless numbers, σ_c is the surface tension for a clean interface, and g is the acceleration due to gravity. In (2.1*a*) we have written the Weber number, the ratio of inertial to capillary forces, as $Re\,Ca$, where Re is the Reynolds number ($Re = \rho Q/a\mu$). Throughout this paper, the surface surfactant concentration is made dimensionless with Γ_0, and all other variables are non-dimensionalized using a, Q, and σ_c.

Equations (2.1*a*) and (2.1*b*) are subject to the following boundary conditions. We prescribe the shape of the surface by $r(s,\ t)$ and $z(s,\ t)$, where s is the arc length measured from the apex (see figure 1), and r and z are the cylindrical coordinates of a point on the surface. At the bubble surface, the stress satisfies

$$\boldsymbol{T}\cdot\boldsymbol{n} + p_g\boldsymbol{n} = \boldsymbol{n}(\sigma\nabla\cdot\boldsymbol{n} - zBo) - \boldsymbol{s}\frac{\partial\sigma}{\partial s}. \tag{2.1c}$$

Here, p_g is the gas pressure relative to the liquid pressure $p(r \to \infty,\ z = 0)$, $\boldsymbol{n}$ and $\boldsymbol{s}$ are the unit normal and tangential vectors defined in figure 1, σ is the dimensionless surface tension, and $\nabla\cdot\boldsymbol{n}$ is the mean curvature. The gas is effectively inviscid, massless and incompressible, so only its pressure appears in (2.1*c*). Equation (2.1*c*) states that the jump in the normal stress is due to the capillary pressure and the difference in the hydrostatic pressures, and that the shear stress exerted by the liquid is balanced by a surface tension gradient. Further, at the bubble surface the fluid velocity satisfies the

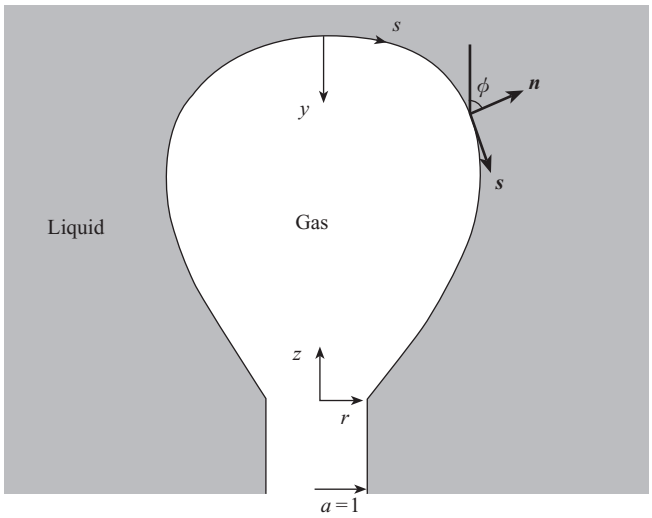

FIGURE 1. A sketch of an axisymmetric bubble pinned at the tip of a capillary with unit radius and zero wall thickness.

constant flow rate condition:

$$\iint_{\Omega_B} \boldsymbol{u}\cdot\boldsymbol{n}\,\mathrm{d}S = \pm 1. \tag{2.1d}$$

The surface integral is over the bubble surface Ω_B. The positive sign holds for bubble expansion, and the negative sign for bubble contraction. Equation (2.1d) determines the unknown gas pressure $p_g = p_g(t)$ as shown in § 4.

On the tube surface, the fluid obeys the no-slip condition:

$$\boldsymbol{u} = 0. \tag{2.1e}$$

At infinity, the fluid is at rest,

$$\boldsymbol{u} = 0, \quad \boldsymbol{T} = 0. \tag{2.1f,g}$$

The surfactant concentration (Γ) affects the surface tension, and they are related here by the Volmer equation of state (Gaines 1966; Aveyard & Haydon 1973):

$$\sigma = 1 - \frac{Ek\Gamma}{1-k\Gamma}, \quad E = \frac{R_u T \Gamma_\infty}{\sigma_c}, \quad k = \frac{\Gamma_0}{\Gamma_\infty}, \tag{2.2a–c}$$

where R_u is the universal gas constant, T is the absolute temperature, Γ_∞ is the surfactant surface concentration at closest packing, E is a dimensionless material constant, and k is the initial concentration made dimensionless by the closest packing concentration. The Volmer equation accounts for the finite size of the surfactant molecules and imposes an upper bound on the surfactant concentration. The material constant E is set to 0.3 throughout this work. Typically, $\Gamma_\infty \approx 5\,\mathrm{molecule/nm^2}$ for unbranched single hydrocarbon surfactants with hydroxyl or carboxylic polar groups (Gaines 1966; Aveyard & Haydon 1973). Thus, if the liquid is water, $\sigma_c = 72.5\,\mathrm{mN/m}$, then $E = 0.3$ at the room temperature of 300 K. To maintain positive σ for $E = 0.3$, we need $0 \leqslant k\Gamma < 0.77$.

The Gibbs elasticity for an insoluble monolayer is $-\Gamma\,\partial\sigma/\partial\Gamma$. We use G to represent the Gibbs elasticity at the initial surfactant concentration ($\Gamma = 1$). The Volmer

equation of state then gives

$$G = -\left(\frac{\partial \sigma}{\partial \Gamma}\right)_{\Gamma=1} = \frac{Ek}{(1-k)^2}. \tag{2.2d}$$

This parameter reflects the variation of surface tension owing to a change in surfactant concentration. Since $E = 0.3$, $G = G(k)$ only.

With the equation of state (2.2*a*) and the Gibbs elasticity (2.2*d*), the tangential stress balance becomes

$$Ca\, \boldsymbol{n} \cdot [\nabla \boldsymbol{u} + \nabla \boldsymbol{u}^t] \cdot \boldsymbol{s} = G(k) \left[\frac{(1-k)^2}{(1-k\Gamma)^2}\right] \frac{\partial \Gamma}{\partial s}. \tag{2.3a}$$

The Marangoni number is $M = G/Ca$, which determines the type of boundary conditions that the liquid flow must satisfy at the bubble surface. As $M \to 0$, the surfactant has no effect on the liquid flow and the zero-stress condition applies at the interface. As $M \to \infty$, (2.3*a*) gives $\partial \Gamma / \partial s \to 0$, which imposes the no-slip condition on the bubble surface. For $0 \leqslant M < \infty$, the surfactant surface concentration is not uniform; its distribution is governed by the conservation equation (Scriven 1960; Waxman 1984; Slattery 1990; Wong *et al.* 1996)

$$\left[\frac{\partial \Gamma}{\partial t}\right]_{\boldsymbol{n}} + \Gamma u_n \nabla \cdot \boldsymbol{n} + \Gamma \nabla_s \cdot \boldsymbol{u}_s + \boldsymbol{u}_s \cdot \nabla_s \Gamma = 0, \tag{2.3b}$$

where u_n is the normal component of the surface velocity, $\boldsymbol{u}_s = (\boldsymbol{u} \cdot \boldsymbol{s})\, \boldsymbol{s}$ is the tangential fluid velocity, and the time derivative is taken along the direction normal to the surface, i.e. keeping the 'fixed' surface coordinates constant (Wong *et al.* 1996). Since $\boldsymbol{u}_s = 0$ at the apex and the needle, $\partial \Gamma / \partial s$ being finite at those points is sufficient to solve (2.3*b*). In (2.3*b*), surface diffusion of the insoluble surfactant has been neglected because surface Péclet numbers are much larger than one. ($Pe_s = Q/aD_s$, where D_s is the surface diffusion coefficient. For a characteristic surface diffusion coefficient of $10^{-6}\,\mathrm{cm}^2/\mathrm{s}$ (see Agrawal & Neuman 1988) and a tube radius of 1 mm, $Pe_s = 10^4$ for Q as small as $1\,\mathrm{mm}^3/\mathrm{s}$.)

Given an instantaneous bubble shape, (2.1)–(2.3) yield the liquid velocity and stress fields, the gas pressure, and the surfactant concentration. The bubble surface advances normally by the kinematic condition:

$$\frac{\mathrm{d}\boldsymbol{X}}{\mathrm{d}t} = (\boldsymbol{u} \cdot \boldsymbol{n})\, \boldsymbol{n}, \tag{2.4}$$

where $\boldsymbol{X}$ is the position of the bubble surface and $\mathrm{d}/\mathrm{d}t$ is the derivative in the Lagrangian frame. During bubble deformation, the bubble is pinned to the outer edge of the tube. Thus, the contact angle is unspecified and is free to take any value as determined by the solution of the problem.

3. Asymptotic solution in the limit $Ca \to 0$

Since most of the experiments are carried out at $Ca \ll 1$, we seek an asymptotic solution in the limit $Ca \to 0$. The zero-order solution shows that at each instant in time the deforming bubble takes the static shape. The surfactant distribution on the bubble surface is uniform, but its value varies with time. Since the bubble shape is

known, the free-boundary nature of this problem is eliminated in the limit $Ca \to 0$. The motion of the bubble can therefore be determined at any later time t, without using the information of bubble evolution before t. This asymptotic solution holds for $Re = o(Ca^{-1})$ and $G \gg Ca$ (or $M \to \infty$).

Consider a regular expansion of the governing equations (2.1)–(2.3) in Ca with k or $G(k) \neq 0$, finite Re, and arbitrary Bo. The momentum equation (2.1a) gives, to leading order, $\nabla p_{[0]} = -Bo\, \boldsymbol{e}_z$ or

$$p_{[0]} = -zBo. \tag{3.1}$$

(Bracketed subscripts denote the order of the expansion in Ca.) Thus, the liquid pressure to leading order is hydrostatic. On the bubble surface, the balance in the normal (2.1c) and tangential (2.3a) stresses becomes

$$p_{g[0]} = \sigma_{[0]} \nabla \cdot \boldsymbol{n}_{[0]} - zBo, \tag{3.2}$$

$$\frac{\partial \Gamma_{[0]}}{\partial s} = 0. \tag{3.3}$$

Equation (3.3) specifies that, to leading order, the surface surfactant concentration is uniform over the bubble surface. Thus, the surface tension is uniform, as governed by the constitutive equation (2.2a):

$$\sigma_{[0]} = 1 - G(k)\frac{(1-k)^2\Gamma_{[0]}}{1-k\Gamma_{[0]}}. \tag{3.4}$$

Equation (3.2) states that, to leading order, the bubble retains the static shape with a uniform surface tension. As the bubble expands or contracts, the surfactant concentration and therefore the surface tension varies with time because the surfactant is insoluble and the total surfactant mass is conserved.

The rate of change of surfactant concentration is governed by the surfactant transport equation (2.3b):

$$\frac{1}{\Gamma_{[0]}}\frac{\mathrm{d}\Gamma_{[0]}}{\mathrm{d}t} + u_{n[0]} \nabla \cdot \boldsymbol{n}_{[0]} + \frac{1}{r_{[0]}}\frac{\partial}{\partial s}[r_{[0]} u_{s[0]}] = 0. \tag{3.5}$$

Here, the time derivative is ordinary because Γ is uniform. Let $A_{[0]}$ be the bubble area to leading order. Multiplying (3.5) by $2\pi r_{[0]}$, and integrating from $s = 0$ to $s_{f[0]}$ with the conditions that $u_{s[0]} = 0$ at $s = 0$ (the bubble apex) and at $s = s_{f[0]}$ (the rim of the tube) leads to the overall balance:

$$\frac{1}{\Gamma_{[0]}}\frac{\mathrm{d}\Gamma_{[0]}}{\mathrm{d}t} = -\frac{2\pi}{A_{[0]}}\int_0^{s_{f[0]}} u_{n[0]} \nabla \cdot \boldsymbol{n}_{[0]} r_{[0]}\, \mathrm{d}s = -\frac{1}{A_{[0]}}\frac{\mathrm{d}A_{[0]}}{\mathrm{d}t}. \tag{3.6}$$

This can be rewritten as

$$\frac{\mathrm{d}}{\mathrm{d}t}[A_{[0]}\Gamma_{[0]}] = 0 \quad \text{or} \quad A_{[0]}\Gamma_{[0]} = m, \tag{3.7}$$

which says that the total surfactant mass is conserved. The dimensionless total mass m is also the initial surface area because $\Gamma_{[0]} = 1$ at $t = 0$.

Given, at $t = 0$, a static bubble coated with a prescribed amount of an insoluble Volmer surfactant, we know Bo, m, k (and therefore $G(k)$), and the initial bubble volume V_0. Equation (3.4) then gives the initial surface tension and (3.2) yields the initial gas pressure. The bubble volume either increases (expansion) or decreases

(contraction) at a constant rate, according to (2.1*d*):

$$\frac{\mathrm{d}V_{[0]}}{\mathrm{d}t} = 2\pi \int_0^{s_{f[0]}} r_{[0]} u_{n[0]}\, \mathrm{d}s = \pm 1. \tag{3.8}$$

Thus, at time t, the bubble volume is

$$V_{[0]} = V_0 \pm t. \tag{3.9}$$

At any given time or bubble volume, we calculate iteratively the bubble shape, $A_{[0]}$, $p_{g[0]}$, $\sigma_{[0]}$ and $\Gamma_{[0]}$ using (3.2), (3.4), and (3.7) (see the Appendix for details). All these variables depend on time only implicitly through $V_{[0]}(t)$. The remaining variables to be determined are $\mathrm{d}\Gamma_{[0]}/\mathrm{d}t$, $u_{n[0]}$, and $u_{s[0]}$. The first two are found by considering the variation of bubble shape in time, subject to the constraints on $\mathrm{d}\Gamma_{[0]}/\mathrm{d}t$ in (3.6) and on $u_{n[0]}$ in (3.8), and by imposing the kinematic condition:

$$\frac{\mathrm{d}\boldsymbol{X}_{[0]}}{\mathrm{d}t} = u_{n[0]} \boldsymbol{n}_{[0]}. \tag{3.10}$$

Again, these variables depend on time only implicitly through the volume $V_{[0]}(t)$. The details are described in the Appendix.

With $r_{[0]}$, $\Gamma_{[0]}$, $\nabla \cdot \boldsymbol{n}_{[0]}$, $\mathrm{d}\Gamma_{[0]}/\mathrm{d}t$, and $u_{n[0]}$ known, the tangential surface velocity $u_{s[0]}$ is found from (3.5) together with the symmetry condition at the bubble apex:

$$u_{s[0]} = 0 \quad \text{at} \quad s = 0. \tag{3.11}$$

A finite-difference scheme integrates the equation from $s = 0$ to the rim of the tube, and yields $u_{s[0]}$ as a function of arclength s. At the rim of the tube, the integration gives $u_{s[0]} \approx 10^{-6}$ for all the cases calculated here. The fact that the integrated $u_{s[0]}$ is almost zero at the rim confirms the validity of not only $u_{s[0]}$, but also the other variables used in (3.5). The tangential surface velocity varies along the bubble surface to maintain a uniform surfactant concentration and to impose the no-slip boundary condition on the liquid flow. (Because the bubble deforms, no-slip does not imply $u_{s[0]} = 0$, but rather it means that the surface points must shift tangentially to give each surface element the same rate of expansion or contraction.)

The above calculations provide the leading-order bubble shape, gas and liquid pressures, surface surfactant concentration and its rate of variation, and normal and tangential velocities on the bubble surface as $Ca \to 0$. These solutions are determined independently of the bulk liquid flow and therefore they apply equally well to an expanding or contracting drop coated with an insoluble monolayer. To calculate the leading-order velocity in the continuous liquid phase, we consider the next order expansion in Ca of (2.1*a*) which is in terms of the leading-order velocity and first-order pressure:

$$Re \left[\frac{\partial \boldsymbol{u}_{[0]}}{\partial t} + \boldsymbol{u}_{[0]} \cdot \nabla \boldsymbol{u}_{[0]} \right] = -\nabla p_{[1]} + \nabla^2 \boldsymbol{u}_{[0]}. \tag{3.12}$$

Equation (3.12) is subject to matching to the previously determined values of $u_{n[0]}$ and $u_{s[0]}$ on the leading-order Young–Laplace shape. From (3.12) it is clear that even though the tangential and normal velocities on the bubble surface already obtained are valid for finite Reynolds number, the difficult task of obtaining the zero-order flow field in the bulk for finite Reynolds number remains. Alternatively, if $Re \ll 1$, then a boundary integral solution can provide the zero-order flow field in the bulk.

4. Creeping flow boundary integral numerical solution

To compare our asymptotic solution to full numerically exact solutions, we solve the low-Reynolds-number contraction of the bubble for arbitrary Ca. This limit neglects the $Re\,Ca$ term in (2.1a) to arrive at the Stokes equations. We follow the standard procedures and use a boundary-integral formulation to solve the Stokes equations and a finite-difference scheme to solve the surfactant transport equation (Stone & Leal 1990; Milliken, Stone & Leal 1993; Milliken & Leal 1994).

The boundary integral equations that govern the fluid motion are (Pozrikidis 1992)

$$\tfrac{1}{2}Ca\,u_\alpha(\hat{r},\hat{z}) + Ca\iint_{\Omega_B}\boldsymbol{u}\cdot\hat{\boldsymbol{T}}^\alpha\cdot\boldsymbol{n}\,\mathrm{d}S - \iint_{\Omega_T}\hat{\boldsymbol{u}}^\alpha\cdot\boldsymbol{T}\cdot\boldsymbol{n}\,\mathrm{d}S = \iint_{\Omega_B}\hat{\boldsymbol{u}}^\alpha\cdot\left[\boldsymbol{n}(\sigma\nabla\cdot\boldsymbol{n} - zBo - p_g) - \boldsymbol{s}\frac{\partial\sigma}{\partial s}\right]\mathrm{d}S \quad (\alpha = r, z), \tag{4.1}$$

where Ω_B and Ω_T denote the bubble and tube surfaces. $\hat{\boldsymbol{T}}^\alpha$ and $\hat{\boldsymbol{u}}^\alpha$ are the stress and velocity fields induced by a unit-strength ring force located at $(\hat{r},\hat{z})$ and acting in direction $\boldsymbol{e}_\alpha, \alpha = r, z$. (They are listed in Appendix A of Wong *et al.* (1998).) At each timestep the bubble shape and surfactant concentration are specified, so that the right-hand side of (4.1) is known, except for the gas pressure. Thus, the unknowns are the fluid velocity on the bubble surface $\boldsymbol{u} = u_r\boldsymbol{e}_r + u_z\boldsymbol{e}_z$, the stress on the tube surface $\boldsymbol{T}\cdot\boldsymbol{n} = \boldsymbol{T}\cdot\boldsymbol{e}_r = T_r\boldsymbol{e}_r + T_z\boldsymbol{e}_z$, and the gas pressure p_g. Putting successively $(\hat{r},\hat{z})$ on the bubble surface and on the tube surface yields two equations when $\alpha = r$, and another two equations when $\alpha = z$. The gas pressure controls the bubble growth rate and vice versa. Thus, p_g is determined by the constant flow rate condition (2.1d). We have five equations for the five unknowns.

We solve the boundary integral equations using Nystrom's method. Each integral is expressed as a sum through the use of Gauss–Legendre quadrature. Putting the source point on the quadrature points successively generates a system of algebraic equations. These equations, together with the discretized constant flow rate condition, are sufficient to determine all the unknowns. For most of the simulations in this paper, 35 points are placed on the tube surface, and 32 on the bubble surface. Convergence tests using more points indicate a relative error of at most 1 % for these numbers of points. Details on the implementation of the Nystrom method are given in Wong *et al.* (1998), which studies the expansion and contraction of a clean bubble.

Given a bubble shape and a surfactant distribution at time t, the boundary integral solution yields the normal and tangential velocity components on the bubble surface. These are then substituted into the surfactant equation (2.3b), along with the mean curvature (known from the shape) and a first-order finite-difference evaluation of the surfactant gradient, to calculate $[\partial\Gamma/\partial t]_{\boldsymbol{n}}$ at time t. Through a second-order Runge–Kutta scheme, the bubble is then advanced at each point on the surface by a distance $u_n\Delta t$ normal to the surface, and Γ is found at the advanced surface points from $[\partial\Gamma/\partial t]_{\boldsymbol{n}}$. For numerical stability, the maximum normal displacement Δn is fixed at each timestep, and is found to depend on Ca. This determines the timestep $\Delta t = \Delta n/u_n^{max}$, where u_n^{max} is the maximum normal velocity at the bubble surface at time t. For the smallest value of Ca calculated ($Ca = 0.02$), $\Delta n = 5\times10^{-5}$, and for the largest value ($Ca = 0.5$), $\Delta n = 2.5\times10^{-3}$. With the bubble shape and surfactant distribution known at time $t+\Delta t$, the solution procedure is repeated.

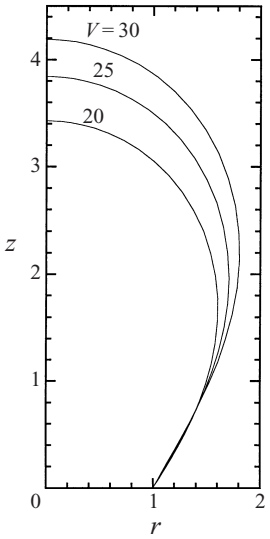

FIGURE 2. Contraction of a bubble from $V = 30$ to 20. $Bo = 0.1$, $Ca = 0.1$, $k = 0.2$. Thus, $G = 0.09375$ and $M = 0.9375$.

5. Results

The Marangoni number $M = G/Ca$ determines the boundary condition at the bubble surface, as shown by the tangential stress balance (2.3*a*). For $M \to 0$ ($G \to 0$, Ca finite), such as the case for a clean bubble, the fluid satisfies zero stress at the bubble surface. For $M \to \infty$ ($Ca \to 0$, G finite), (2.3*a*) gives $\partial \Gamma / \partial s = 0$, and the surfactant transport equation specifies the tangential velocity on the bubble surface (§ 3). The purpose of this section is to illustrate the transition between the two limits. The boundary integral results at high M agree with the asymptotic solution in § 3. The agreement confirms both solutions.

This section studies bubble contraction from bubble volume $V = 30$ to 20 at $Bo = 0.1$ to illustrate the transition. The behaviour of this contracting bubble is controlled by two parameters: Ca and k. Once a value is assigned to these parameters, we can calculate $G = G(k)$ from (2.2*d*) and $M = G/Ca$. Results for a specific set of parameters ($Ca = 0.1$, $k = 0.2$) are presented first to illustrate the general features. The bubble shapes during contraction are shown in figure 2. A contracting bubble satisfies $\mathrm{d}V/\mathrm{d}t = -1$, so $V = 30 - t$ and the bubble takes 10 units of time to shrink to $V = 20$. The clean bubble calculations of Wong *et al.* (1998) demonstrate that for $Ca \leqslant 0.1$ viscous stresses do not distort the bubble shape from the Young–Laplace solution during expansion or contraction, except near the beginning for $t \sim Ca$ (see below). Likewise, the contracting shapes in figure 2 deviate only slightly from Young–Laplace solutions with identical volumes and a uniform surface tension corresponding to the mean tension at that bubble area. As shown below, the surface concentration is not uniform. The congruence to uniform tension Young–Laplace shapes indicates that the surface tension inhomogeneity does not have a noticeable effect on the shape for the chosen set of parameters.

For $Ca \ll 1$, capillarity dominates throughout bubble contraction, except near $t = 0$ where viscous forces dominate. At $t < 0$, the capillary pressure balances exactly the pressure difference across the static bubble surface. At $t = 0$, the gas pressure is decreased instantaneously by Δp to effect bubble contraction at a unit flow rate. At

that instant, the bubble shape remains the same, so that the capillary pressure is the same and still exactly balances the initial gas pressure. Therefore, the pressure drop Δp can only be balanced by the viscous normal stress. Thus, the motion at $t = 0$ corresponds to a bubble with zero surface tension even in the limit $Ca \to 0$. This singular region is typical of start-up problems and exists for $t \sim Ca$ (Wong *et al.* 1998).

This singular region is reflected in the normal and tangential surface velocities plotted in figures 3(*a*) and 3(*b*). The normal velocity u_n at $t = 0$ shows a different trend from the velocity profiles at later times owing to the start-up singularity. For $t \geqslant 1$, the singularity has ended, and u_n is essentially determined at this small Ca (0.1) by the kinematic constraint of contraction of the Young–Laplace pendant shape. As such, $|u_n|$ is always highest at the apex and decreases to zero at the base ($z = 0$), although not always monotonically. For example, $u_n > 0$ near the base, i.e. moving outward, despite the fact that the bubble is contracting. This is because the static bubble shape changes from pendant to spherical as a bubble shrinks and gravity becomes less important; the interface near the base must move outward to achieve this shape change. Finally, at times later than shown, u_n becomes linear in z as the bubble becomes more spherical (Wong *et al.* 1998).

The tangential velocity u_s (figure 3(*b*)) shows a ten-fold increase in magnitude during this contraction. At $t = 0$, the start-up singularity gives a u_s as if the bubble has zero surface tension. At $t = 1$, the start-up singularity has dissipated, but the surfactant distribution is not perturbed sufficiently to generate a significant concentration gradient (see figure 4). Therefore, u_s at $t = 1$ can be taken as the tangential velocity for a clean bubble. From $t = 1$ to 10, u_s increases by roughly 2.5 times. However, u_s for a clean bubble remains at the same level at $t = 10$ as at $t = 1$, as shown later in figure 9(*b*) (note the magnitude at $t = 10$ for the case $k = 0$). Thus, the large increase in u_s from $t = 1$ to 10 is due to the presence of surfactant.

This large increase in u_s is investigated. The tangential velocity is positive, which means that the surface flow is from the bubble apex towards the base (figure 3(*b*)). Intuitively, one would predict that the surfactant will therefore be convected towards the base and accumulated there. However, a plot of the surfactant concentration in figure 4 shows that the concentration is actually higher at the apex. A careful comparison of the terms in the conservation equation (2.3*b*) reveals that the local area compression term $u_n \nabla \cdot \boldsymbol{n}$ always dominates the convective terms $\Gamma \nabla_s \cdot \boldsymbol{u}_s + \boldsymbol{u}_s \cdot \nabla_s \Gamma$. Since u_n is always highest at the apex, the surface compression is highest there. The high compression increases the surfactant concentration, and the convection towards the base is not fast enough to remove this excess. As a result, Γ is higher at the apex, and the surface tension σ is lower there (σ is related to Γ by (2.2*a*)). The Marangoni force acts to pull surface fluid from the apex towards the base, and enhances the tangential flow. This explains the increase in tangential flow when a surfactant is present.

The surfactant concentrations in figure 4 also exhibit an overall increase in magnitude with time. This is due to the contraction of the total bubble area. As shown in figure 5, the area shrinks by roughly 20 % in 10 time units. Also plotted in figure 5 is the gas pressure, which increases with time because the capillary pressure increases as the bubble shrinks from $V = 30$ to 20.

The Marangoni number determines the boundary condition at the bubble surface and affects the flow behaviour. Its effect is studied by conducting two series of numerical simulations of contracting a bubble from $V = 30$ to 20 at $Bo = 0.1$. In the first, k is fixed at 0.2, and Ca is decreased from 0.5 to 0.02. The Marangoni number M therefore varies from 0.2 to 5, and the results are presented in figures 6, 7 and

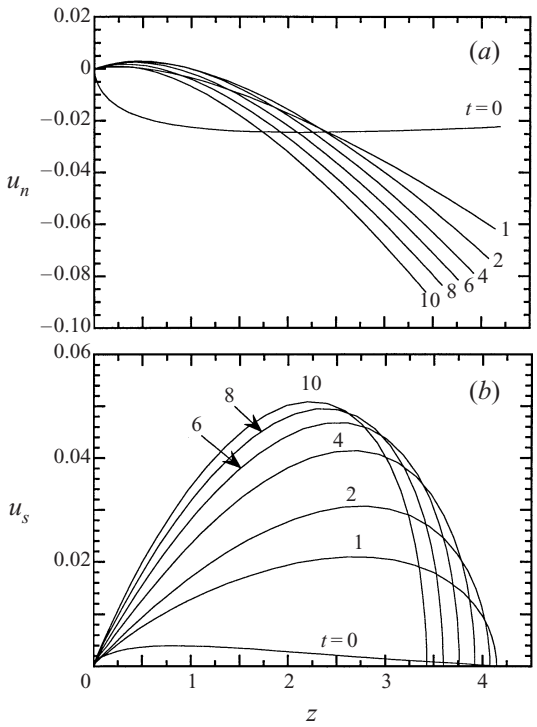

FIGURE 3. The (*a*) normal and (*b*) tangential surface velocities versus the vertical distance z at different times. $Bo = 0.1$, $Ca = 0.1$, $k = 0.2$. Thus, $G = 0.09375$ and $M = 0.9375$.

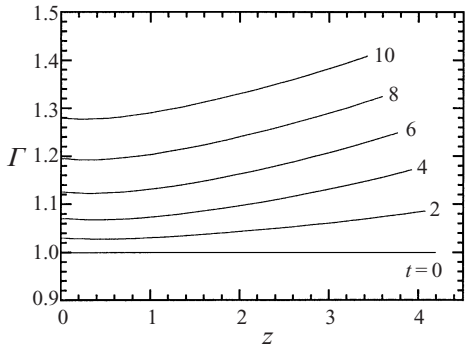

FIGURE 4. Surfactant concentration versus the vertical distance z at different times. $Bo = 0.1$, $Ca = 0.1$, $k = 0.2$. Thus, $G = 0.09375$ and $M = 0.9375$.

8. Figure 6 shows the gas pressure p_g versus time for different Ca. For each Ca, p_g increases with time owing to the increase in capillary pressure as the bubble shrinks from $V = 30$ to 20. The overall level of p_g increases as Ca decreases because a higher gas pressure is needed to balance the capillary pressure as the viscous normal stress drops. As Ca decreases, p_g approaches the asymptotic solution $p_{g[0]}$ for $Ca = 0$ described in § 3. The agreement between the numerical and asymptotic solutions serves as a mutual check for both solutions.

The normal and tangential surface velocities at $t = 10$ or $V = 20$ are presented in figure 7 for different Ca. It shows that the normal velocity is insensitive to Ca for

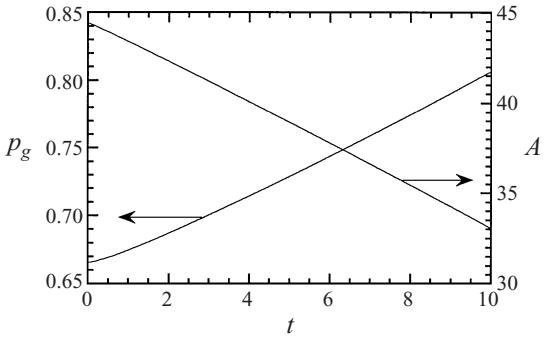

FIGURE 5. The gas pressure and bubble area versus time. $Bo = 0.1$, $Ca = 0.1$, $k = 0.2$. Thus, $G = 0.09375$ and $M = 0.9375$.

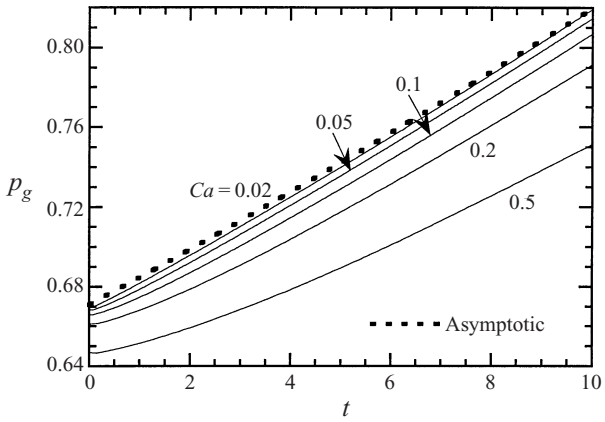

FIGURE 6. The gas pressure versus time for different Ca or M $(= G/Ca)$. $Bo = 0.1$, $k = 0.2$ and thus $G = 0.09375$.

$Ca < 0.2$; the velocity profile for $Ca = 0.02$ already coincides with the asymptotic solution for $Ca = 0$. As explained in the asymptotic theory (§ 3), u_n is determined from the kinematic condition, which depends mainly on the bubble shape. For $Ca \leqslant 0.1$, the bubble takes nearly Young–Laplace shapes for $Ca = 0$ (Wong *et al.* 1998). Thus, u_n is insensitive to Ca.

Figure 7 (*b*) shows that the tangential velocity u_s varies non-monotonically with Ca. As Ca decreases, the maximum value of u_s increases and reaches a maximum around $Ca = 0.1$ ($M \approx 1$), before decreasing slightly to the asymptotic solution. The agreement with the asymptotic solution is again noteworthy because the two solutions are obtained by two very different avenues; the boundary integral method determines the tangential velocity from the fluid flow, whereas the asymptotic solution calculates it directly from the surfactant transport equation.

The surfactant concentration Γ at $V = 20$ is plotted in figure 8 for several Ca ranging from 0.02 to 0.5. It shows that as Ca decreases, Γ becomes more uniform, because the viscous shear stress is weaker and can only sustain a smaller surface tension gradient. The dashed curve in figure 8 is the uniform asymptotic solution for $Ca = 0$ determined from the global mass conservation (3.7). The boundary integral solutions merge towards this uniform asymptotic value as Ca decreases. As described in § 2, the boundary integral solutions are determined without imposing the global

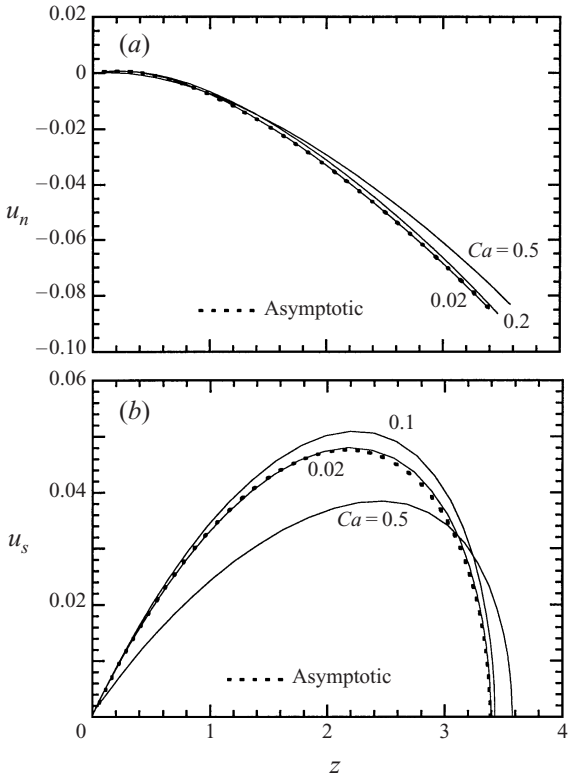

FIGURE 7. The (*a*) normal and (*b*) tangential surface velocities versus the vertical distance z for different Ca or M $(= G/Ca)$ at $t = 10$ or $V = 20$. $Bo = 0.1$, $k = 0.2$ and thus $G = 0.09375$.

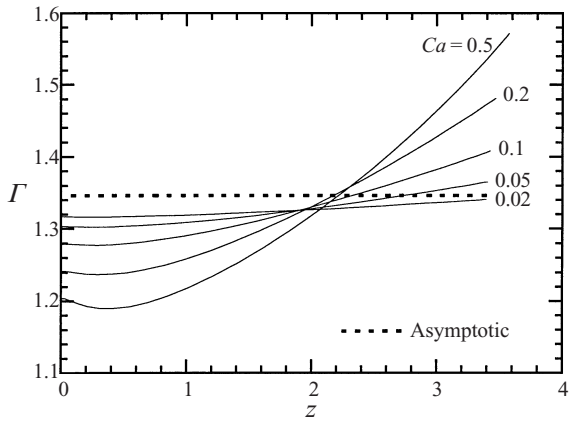

FIGURE 8. Surfactant concentration versus the vertical distance z for different Ca or M $(= G/Ca)$ at $t = 10$ or $V = 20$. $Bo = 0.1$, $k = 0.2$ and thus $G = 0.09375$.

conservation of surfactant mass, and mass leakage is possible owing to discretization errors. This accounts for the difference shown in figure 8 between the level of concentration at $Ca = 0.02$ and the asymptotic curve. Mass leakage ranges from 0.8 % for $Ca = 0.5$ to 1.5 % for $Ca = 0.02$. This leakage decreases as a finer grid size is used.

In the second series of numerical simulation, the bubble is again contracted from

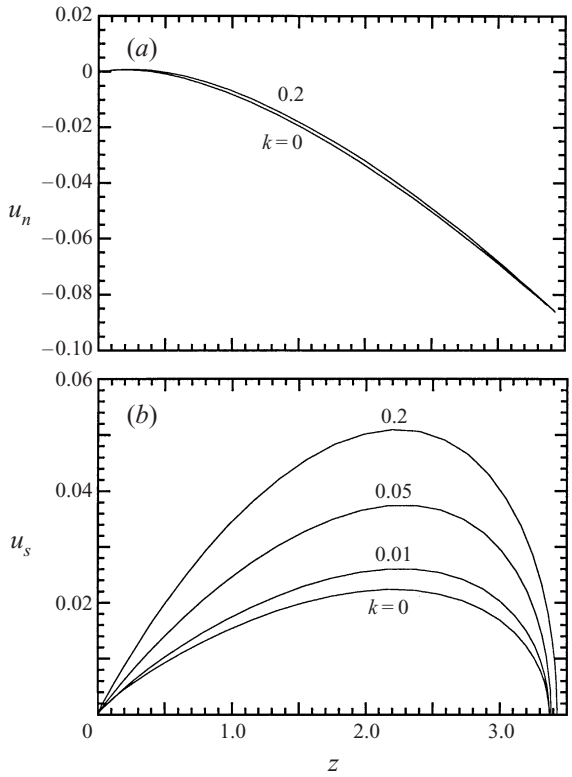

FIGURE 9. The (*a*) normal and (*b*) tangential surface velocities versus the vertical distance z at $t = 10$ or $V = 20$ for $k = 0$, 0.01, 0.05 and 0.2. The corresponding values of $G(k)$ are 0, 0.003, 0.017, and 0.09375. $Bo = 0.1$, $Ca = 0.1$.

$V = 30$ to 20 at $Bo = 0.1$. Results at $V = 20$ are presented in figures 9 and 10 for $Ca = 0.1$, and $k = 0$ to 0.2. According to the definition of k in (2.2*c*), increasing k means adding more surfactant to the bubble surface. In figure 9, u_n and u_s are plotted against the vertical position for various k. The data show that k has surprisingly little effect on u_n. At $Ca = 0.1$, the bubble shapes are essentially Young–Laplace (Wong *et al.* 1998). Since u_n derives from the shape, the normal velocity is not affected. The tangential velocity u_s, however, increases by almost 2.5 fold as k increases from 0 to 0.2 or equivalently as M increases from 0 to 0.9375. This again confirms that the Marangoni force significantly enhances the tangential flow. The value $M = 0.9375$ is sufficient to reveal the full effect of the Marangoni force, since the magnitude of u_s at $M = 0.9375$ is about the same as the asymptotic solution for $M \to \infty$ depicted in figure 7(*b*).

As k increases, more surfactant is added, so that the surface tension drops and a gradient in surface tension is possible, as shown in figure 10(*a*). This gradient is responsible for enhancing the tangential flow. Figure 10(*b*) presents the surfactant concentration Γ as a function of the vertical position for various k. As k increases, Γ becomes more uniform because of the higher tangential flow that redistributes the surfactant from the bubble apex to the base. The surface tension becomes less uniform as Γ becomes more uniform because the elasticity of the surfactant increases. (As k increases from 0 to 0.2, the elasticity number G defined in (2.2*d*) varies from 0 to 0.09375.) Note that at $k = 0$, $G = 0$, so the surfactant does not affect the surface

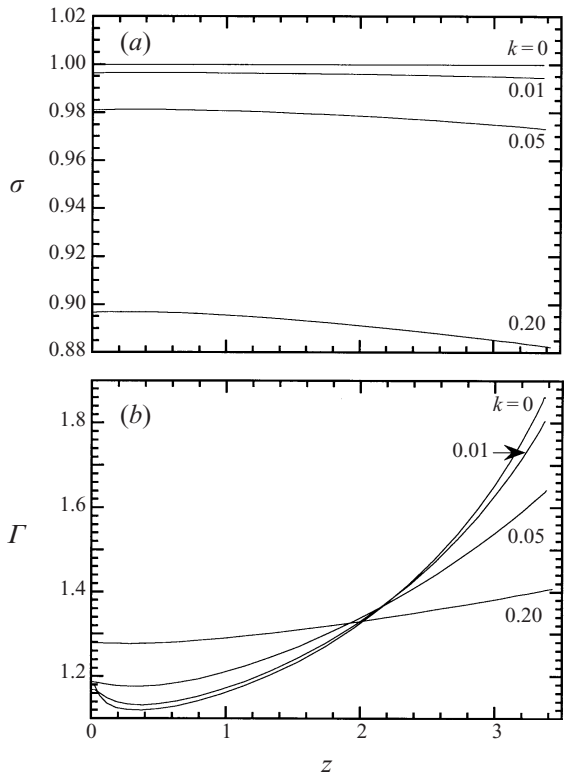

FIGURE 10. (*a*) Surface tension and (*b*) surfactant concentration versus the vertical distance at $t = 10$ for $k = 0$, 0.01, 0.05 and 0.2. The corresponding values of $G(k)$ are 0, 0.003, 0.017 and 0.09375. $Bo = 0.1$, $Ca = 0.1$.

tension; the surfactant is simply being compressed and convected along the surface. The surface velocities for $k = 0$ are therefore the same as for a clean interface, and the distribution holds for a passively adsorbed species. Note that because Γ is made dimensionless by Γ_0, $k = 0$ is only meant in the limiting sense.

Throughout this paper, results of u_n, u_s, σ and Γ are plotted against the vertical distance z instead of the arclength s because it is easier to see the relative position on the bubble. At the bubble apex $s = 0$, u_n, σ and Γ have finite slopes when plotted against z, and thus will satisfy $\partial/\partial s = 0$ because $\partial/\partial s = (\partial z/\partial s)\partial/\partial z$ and $\partial z/\partial s = 0$ at $s = 0$. Only u_s exhibits unbounded slopes at $s = 0$. In this case, it can be shown using the surfactant mass balance (2.3*b*) that as $s \to 0$, $\partial u_s/\partial s \to -(\Gamma^{-1}\partial\Gamma/\partial t + \frac{1}{2}u_n\nabla\cdot\boldsymbol{n})$, i.e. the slope $\partial u_s/\partial s$ approaches a constant near the apex. Values of this slope are listed in Table 1 for all the cases studied in figures 3 (*b*), 7 (*b*) and 9 (*b*).

6. Extension to bulk soluble surfactants

Our conclusions of uniform concentration and large tangential velocity during bubble expansion or contraction have been obtained assuming that the surfactant is insoluble. An important issue is how surfactant exchange between the surface and the liquid affects these conclusions, since most applications of the bubble expansion or contraction methods aim to measure kinetic and diffusive transport coefficients. To discuss this influence, we assume that the concentration of the bulk soluble

Ca	k	t	$\frac{\partial u_s}{\partial s}$
0.1	0.2	1	0.01457
0.1	0.2	2	0.02271
0.1	0.2	4	0.03166
0.1	0.2	6	0.03623
0.1	0.2	8	0.03890
0.1	0.2	10	0.04087
0*	0.2	10	0.03658
0.02	0.2	10	0.03819
0.5	0.2	10	0.03352
0.1	0	10	0.01795
0.1	0.01	10	0.02193
0.1	0.05	10	0.03184

* From the asymptotic solution.

TABLE 1. Tangential velocity gradient at the bubble apex $s = 0$. $Bo = 0.1$.

surfactant far from the bubble surface is equal to C_0. In the absence of interactions among adsorbed molecules, kinetic exchange of a bulk soluble surfactant between the air/water surface and the aqueous sublayer immediately adjoining the interface obeys a Langmuir relation (Baret 1969; Borwankar & Wasan 1983):

$$\frac{q}{\alpha\Gamma_0} = \left[\frac{\beta C_0}{\alpha}\left(\frac{1}{k} - \Gamma\right) C_s - \Gamma\right], \tag{6.1}$$

where q is the dimensional kinetic flux, C_s is the concentration (non-dimensionalized by C_0) in the liquid sublayer adjacent to the bubble, α and β are, respectively, the kinetic rate constants for desorption and adsorption, Γ_0 is the surface concentration in equilibrium with C_0, Γ is the non-dimensional surface concentration (non-dimensionalized by Γ_0), and $k = \Gamma_0/\Gamma_\infty$ is the ratio of the equilibrium adsorption to the maximum packing concentration (Γ_∞). At equilibrium, $\Gamma = 1$, $C_s = 1$, and $q = 0$. Thus, (6.1) gives $k = (1 + \alpha/\beta C_0)^{-1}$. This and the Gibbs–Duhem equation derive the equation of state for the surface tension σ (made dimensionless by the clean tension):

$$\sigma = 1 - \frac{G_s(k)(1-k)}{k}\ln(1 - k\Gamma), \tag{6.2}$$

where $G_s(k) = Ek/(1-k)$ is the Gibbs elasticity of the soluble surfactant evaluated at the equilibrium coverage, and E is as before. The tangential stress balance becomes

$$Ca\, \boldsymbol{n} \cdot \left[\nabla \boldsymbol{u} + \nabla \boldsymbol{u}^t\right] \cdot \boldsymbol{s} = G_s(k)\frac{1-k}{1-k\Gamma}\frac{\partial \Gamma}{\partial s}. \tag{6.3}$$

The Marangoni number for the soluble surfactant problem is $M_s = G_s/Ca$. To complete the formulation of this problem, the kinetic rate q contributes an additional term to the left-hand side of the surface conservation equation (2.3b), and this rate is also equated to the diffusive flux to the surface to provide a boundary condition at the bubble surface for the unsteady convective diffusion equation.

Consider the case of contraction. For any non-zero value of M_s, the gradient in surface concentration created by the non-uniformity in the local area compression is reduced by kinetic and diffusive transport into the bulk. Thus, the Marangoni force is reduced and so is the tangential surface velocity. We expect, therefore, that as the

surface contracts, the tangential velocity will be smaller for a soluble surfactant than for an insoluble one with comparable Marangoni numbers.

In the limit $Ca \to 0$ or $M_s \to \infty$, (6.3) also requires the leading-order surface concentration to be uniform. Thus, the uniformity of the surface concentration in this limit is unaffected by the surfactant solubility. However, for the soluble case, the total amount of surfactant on the bubble surface changes as the area changes. The tangential surface velocity needed to maintain the surface concentration uniform is governed by the conservation equation, and we examine its form below, first for kinetic and then for diffusion-limited mass transfer.

For kinetically controlled transport, diffusion between the sublayer and the bulk is much faster than the kinetic transport between the sublayer and the surface. Thus, the sublayer concentration is always equal to the far field equilibrium value (i.e. $C_s = 1$), and (6.1) gives the dimensionless kinetic flux as $(1 - \Gamma)/(1 - k)$. The augmented conservation equation becomes

$$\frac{\mathrm{d}\Gamma}{\mathrm{d}t} + \Gamma u_n \nabla \cdot \boldsymbol{n} + \frac{\Gamma}{r}\frac{\partial}{\partial s}(u_s r) + \frac{Bi}{1-k}(\Gamma - 1) = 0, \tag{6.4}$$

where Γ is the non-dimensional uniform surface concentration, and the Biot number $Bi = \alpha a^3/Q$ measures the ratio of the kinetic rate for desorption ($\alpha\Gamma_0$) to the rate of change of surface concentration owing to the change in area ($\Gamma_0 Q/a^3$). Note that as in the case of the insoluble surfactant, (6.4) combined with the efficient method described in § 3 can easily be solved to obtain the tangential surface velocity without recourse to the equations of motion. As such, its range of validity is equally broad.

If $Bi \gg 1$, then a regime arises in which the large kinetic exchange and the large elasticity compete with one another to determine the surface tangential velocity. If we reconsider our asymptotic expansion in $Ca \to 0$ in § 3 and assume $Bi = \lambda Ca^{-1}$, where λ is a constant independent of Ca, then (6.4) to leading order in Ca yields $\Gamma_{[0]} = 1$, i.e. the surface concentration takes the equilibrium value and is independent of time. Thus, the calculations of the bubble shape and normal surface velocity are simplified because the surface tension is uniform and independent of time. The (leading-order) tangential surface velocity follows from the first-order equation for the tangential stress and the mass conservation:

$$\boldsymbol{n}_{[0]} \cdot \left[\nabla \boldsymbol{u}_{[0]} + \nabla \boldsymbol{u}_{[0]}^t\right] \cdot \boldsymbol{s}_{[0]} = G(k)\frac{\partial \Gamma_{[1]}}{\partial s}, \tag{6.5}$$

$$u_{n[0]} \nabla \cdot \boldsymbol{n}_{[0]} + \frac{1}{r_{[0]}}\frac{\partial}{\partial s}(u_{s[0]} r_{[0]}) + \frac{\lambda}{1-k}\Gamma_{[1]} = 0. \tag{6.6}$$

Because the tangential stress appears in the equations, these calculations, unlike the order Ca^0, are not divorced from the equations of motion in the liquid. These equations, however, do describe a return to the stress-free condition when the kinetic exchange dominates over the large elasticity effect of increasing the surface tangential velocity. In this latter limit, $Bi \sim Ca^{-2}$ or $\lambda \to \infty$, so that (6.6) gives $\Gamma_{[1]} \to 0$. Equation (6.5) then requires the interface to become stress-free, and thus the surface velocities are the reduced ones for the stress-free condition (as given most closely by $Ca = 0.5$ in figure 7(*b*) where the capillary number is sufficiently large so as to minimize the effect of the Marangoni traction).

If bulk diffusion is rate limiting, then local equilibrium prevails between the surfactant on the surface and in the sublayer, and (6.1) with $q = 0$ gives

$$\Gamma = \frac{C_s}{1 - k + kC_s}. \tag{6.7}$$

Note that in the limit $M_s \to \infty$, this equilibrium condition dictates that $C_{s[0]}$ is uniform along the bubble surface because the surface concentration $\Gamma_{[0]}$ is uniform in this limit. The leading-order surface mass balance becomes the boundary condition at the interface for the bulk diffusion equation. To leading order, the mass balance is

$$\frac{\mathrm{d}\Gamma_{[0]}}{\mathrm{d}t} + \Gamma_{[0]} u_{n[0]} \nabla \cdot \boldsymbol{n}_{[0]} + \frac{\Gamma_{[0]}}{r_{[0]}} \frac{\partial}{\partial s}(u_{s[0]} r_{[0]}) + \frac{aC_0}{\Gamma_0 Pe} \boldsymbol{n}_{[0]} \cdot \nabla C_{[0]} = 0, \tag{6.8}$$

where $Pe\ (= Q/aD)$ is the bulk Péclet number. The coefficient $aC_0/\Gamma_0\, Pe$ is the ratio of the rate of accumulation (DC_0/a) of surfactant on the surface owing to diffusion to the rate of change $(\Gamma_0 Q/a^3)$ of the surface concentration owing to the area change. Once again, if $aC_0/\Gamma_0\, Pe \sim Ca^{-1}$, then $\Gamma_{[0]} = 1$ and $C_{s[0]} = 1$, and the elasticity and the diffusive exchange compete to determine the surface velocity. If $aC_0/\Gamma_0\, Pe \sim Ca^{-2}$, then the surface again becomes tangentially stress free.

In dynamic tension experiments, if either $Bi \gg 1$ or $aC_0/\Gamma_0\, Pe \gg 1$, then the surface concentration and dynamic tension remain to leading order at their equilibrium values. Such experiments are not useful, since they yield no insight into the surfactant transport. To obtain such information, ideal dynamic tension experiments require $Bi \ll 1$ or $aC_0/\Gamma_0\, Pe \leqslant 1$. Thus, the surface concentration of surfactant must change appreciably upon contraction or expansion, and can be accurately measured via the significant changes in dynamic tension. In these regimes, the exchange does not bring the surface back to a stress-free condition, and the surface convection, although not as large as in the insoluble limit, is nonetheless enhanced from the stress-free (clean interface) case.

Although $u_s \sim u_n$, the small penetration depth solutions described in § 1 still hold for time $\ll a^2/D$ when the diffusion boundary layer is thin compared with the tube radius. In this regime, tangential convection is small compared to normal convection, even when the normal and tangential velocities are of the same order because the gradient in surfactant concentration is much smaller in the tangential direction than in the normal direction; use of (1.3) is then valid (Macleod & Radke 1994).

7. Summary

This work studies the contraction or expansion of a bubble from the tip of a tube with an insoluble monolayer adsorbed on its surface. This is a model problem for understanding the hydrodynamics and surfactant distribution in dynamic tension measurement techniques, such as the maximum bubble pressure, drop weight, growing drop, pulsating bubble, and pendant bubble and drop shape analysis methods. We develop asymptotic solutions in the limit $Ca \to 0$ that hold for $Re = o(Ca^{-1})$, non-zero Gibbs elasticity (G), and arbitrary Bond number. This limit is typical of the air/water interface, which is the interface of greatest interest. We establish two important conclusions from the asymptotic solution. (i) Although the larger area shrinkage at the apex during contraction tends to increase the surface concentration there relative to the rim, the large Marangoni force drives a substantial Marangoni convection which reduces this developing gradient and maintains a uniform concentration. (ii) The resulting tangential velocity is higher than that of the clean-bubble case. In addition, we obtain solutions for the surface velocities and surfactant concentration without solution of the bulk flow field. As such, these solutions are valid for hanging drops as well as bubbles formed in a liquid. Full numerical boundary integral solutions for $Re \ll 1$ and arbitrary Ca and G match the asymptotic results as $Ca \to 0$ with G fixed.

The conclusion that the surfactant distribution (and therefore the tension) is

uniform verifies the assumption used in the dynamic surface-tension measurement methods. However, the enhancement of tangential surface convection suggests the need for the refinement of models of surfactant transport, which at the present time include only radial convection and diffusion of surfactant in the bulk liquid.

Appendix. The zero-order solution

Let $(r_{[0]}(s;t),\ y_{[0]}(s;t))$ be the coordinates of the bubble surface to leading order in Ca, with y starting from the bubble apex and pointing downward, i.e. $y_{[0]}(s;t) = h_{[0]}(t) - z_{[0]}(s;t)$, where $h_{[0]}$ is the leading-order bubble height (see figure 1). In these coordinates, the Young–Laplace equation (3.2), which governs the leading-order shape, becomes

$$\nabla \cdot \boldsymbol{n}_{[0]} = \frac{\partial \phi_{[0]}}{\partial s} + \frac{\sin\phi_{[0]}}{r_{[0]}} = \frac{2}{R_{[0]}} - \frac{Bo}{\sigma_{[0]}} y_{[0]}, \tag{A 1}$$

$$\frac{\partial r_{[0]}}{\partial s} = \cos\phi_{[0]}, \tag{A 2}$$

$$\frac{\partial y_{[0]}}{\partial s} = \sin\phi_{[0]}, \tag{A 3}$$

$$p_{g[0]} = \frac{2\sigma_{[0]}}{R_{[0]}} - h_{[0]} Bo, \tag{A 4}$$

where $R_{[0]}$ is the radius of curvature at the apex, and $\phi_{[0]}$ is the angle between the normal and the z-axis (figure 1). The surface tension $\sigma_{[0]}$ is uniform and is related to the surfactant concentration by the constitutive equation (3.4):

$$\sigma_{[0]} = 1 - G(k)\frac{(1-k)^2\Gamma_{[0]}}{1-k\Gamma_{[0]}}. \tag{A 5}$$

The surfactant concentration varies with time to conserve the total surfactant mass:

$$\Gamma_{[0]} A_{[0]} = m, \tag{A 6}$$

$$A_{[0]} = 2\pi \int_0^{s_{f[0]}} r_{[0]}\, \mathrm{d}s. \tag{A 7}$$

At $t = 0$, we are given a value for Bo, k (and therefore $G(k)$), and the bubble shape. From the shape, we can determine $R_{[0]}(0)$, $V_{[0]}(0) = V_0$, and $A_{[0]}(0) = m$ (since $\Gamma_{[0]}(0) = 1$).

Because the bubble shape is known in the limit $Ca \to 0$, the free-boundary nature of the problem is eliminated and the solution can be determined at any time without knowing the history of the evolution. To find the solution at a later time, we first pick a value for $R_{[0]}$, and solve (A 1)–(A 7) by an iterative method. Starting with $\Gamma_{[0]} = 1$, we get an initial guess for $\sigma_{[0]}$ from (A 5), and integrate (A 1)–(A 3) by a fourth-order Runge–Kutta method with the following starting conditions at $s = 0$: $\phi_{[0]} = 0$, $r_{[0]} = 0$, and $y_{[0]} = 0$. The integration is stopped when the radius reaches the tube tip, i.e. when $r_{[0]} = 1$. This determines the total arclength $s_{f[0]}$. The bubble area $A_{[0]}$ is then calculated from (A 7), and is substituted into (A 6) to yield a new $\Gamma_{[0]}$. A new surface tension is again calculated for this new value of $\Gamma_{[0]}$, and a new bubble shape solved, and so on. The solution converges quadratically to an accuracy of 6 significant figures in 4–5 iterations. The converged solution is used to calculate the

volume $V_{[0]}$, which is related to the non-dimensional time by (3.9):

$$V_{[0]} = V_0 \pm t. \tag{A 8}$$

If the volume or time is not the desired one, a new value of $R_{[0]}$ is chosen, and the above procedures are repeated until the right volume or time is obtained. Thus, given a volume or time, we can determine $R_{[0]}$, $\Gamma_{[0]}$, $\sigma_{[0]}$, $A_{[0]}$, and the bubble shape. From the shape, we get $h_{[0]} = y_{[0]}(s_{f[0]})$, which gives $p_{g[0]}$ from (A 4).

The normal surface velocity is given by the kinematic condition (3.10) as $u_{n[0]} = \boldsymbol{n}_{[0]} \cdot (\mathrm{d}\boldsymbol{X}_{[0]}/\mathrm{d}t)$ or

$$u_{n[0]} = \frac{\partial r_{[0]}}{\partial t} \sin\phi_{[0]} + \left(\frac{\mathrm{d}h_{[0]}}{\mathrm{d}t} - \frac{\partial y_{[0]}}{\partial t} \right) \cos\phi_{[0]}. \tag{A 9}$$

This is the normal velocity relative to the tube tip. The unknown $\mathrm{d}h_{[0]}/\mathrm{d}t$ is found indirectly by first solving for the normal velocity relative to the bubble apex:

$$U(s) = \frac{\partial r_{[0]}}{\partial t} \sin\phi_{[0]} - \frac{\partial y_{[0]}}{\partial t} \cos\phi_{[0]}. \tag{A 10}$$

Then, the pinning condition $u_{n[0]} = 0$ at $s = s_{f[0]}$ gives $\mathrm{d}h_{[0]}/\mathrm{d}t$ in terms of $U(s_{f[0]})$, and we recover

$$u_{n[0]} = U(s) - \left[\frac{U(s_{f[0]})}{\cos\phi_{[0]}(s_{f[0]})} \right] \cos\phi_{[0]}. \tag{A 11}$$

To obtain the derivatives of the surface coordinates in (A 10), we differentiate (A 1)–(A 3) with respect to time at constant s:

$$\frac{\partial}{\partial s}\left(\frac{\partial \phi_{[0]}}{\partial t} \right) = \frac{\sin\phi_{[0]}}{r_{[0]}^2} \frac{\partial r_{[0]}}{\partial t} - \frac{Bo}{\sigma_{[0]}} \frac{\partial y_{[0]}}{\partial t} - \frac{\cos\phi_{[0]}}{r_{[0]}} \frac{\partial \phi_{[0]}}{\partial t} - \frac{2}{R_{[0]}^2} \frac{\mathrm{d}R_{[0]}}{\mathrm{d}t} + \frac{y_{[0]} Bo}{\sigma_{[0]}^2} \frac{\mathrm{d}\sigma}{\mathrm{d}\Gamma} \frac{\mathrm{d}\Gamma_{[0]}}{\mathrm{d}t}, \tag{A 12}$$

$$\frac{\partial}{\partial s}\left(\frac{\partial r_{[0]}}{\partial t} \right) = -\sin\phi_{[0]} \frac{\partial \phi_{[0]}}{\partial t}, \tag{A 13}$$

$$\frac{\partial}{\partial s}\left(\frac{\partial y_{[0]}}{\partial t} \right) = \cos\phi_{[0]} \frac{\partial \phi_{[0]}}{\partial t}, \tag{A 14}$$

With $R_{[0]}$, $\Gamma_{[0]}$, and the bubble shape already known from (A 1)–(A 8), there remain three unknown variables: $\partial r_{[0]}/\partial t$, $\partial y_{[0]}/\partial t$, and $\partial \phi_{[0]}/\partial t$. The parameters $\mathrm{d}R_{[0]}/\partial t$ and $\mathrm{d}\Gamma_{[0]}/\mathrm{d}t$ are also unspecified. Thus, two more equations are required to close the system. These are the constant flow rate condition and the integral surfactant mass balance:

$$2\pi \int_0^{s_{f[0]}} u_{n[0]} r_{[0]} \, \mathrm{d}s = \pm 1, \tag{A 15}$$

$$\frac{\mathrm{d}\Gamma_{[0]}}{\mathrm{d}t} + \frac{2\pi\Gamma_{[0]}}{A_{[0]}} \int_0^{s_{f[0]}} u_{n[0]} \nabla \cdot \boldsymbol{n}_{[0]} r_{[0]} \, \mathrm{d}s = 0. \tag{A 16}$$

We solve by first dividing (A 10)–(A 16) by $\mathrm{d}R_{[0]}/\mathrm{d}t$, and seek solutions of the ratio of the unknowns to $\mathrm{d}R_{[0]}/\mathrm{d}t$. This is again done iteratively. Assume a value of $(\mathrm{d}\Gamma_{[0]}/\mathrm{d}t)/(\mathrm{d}R_{[0]}/\mathrm{d}t)$, and integrate (A 12)–(A 14) by a fourth-order Runga–Kutta method with the following starting conditions at $s = 0$: $\partial r_{[0]}/\partial t = 0$, $\partial y_{[0]}/\partial t = 0$, and $\partial \phi_{[0]}/\partial t = 0$. Substitution of the solution into (A 16) with $u_{n[0]}/(\mathrm{d}R_{[0]}/\mathrm{d}t)$ from (A 11)

gives a new value for $(d\Gamma_{[0]}/dt)/(dR_{[0]}/dt)$. This iteration procedure again converges quadratically. After convergence, $(dr_{[0]}/dt)/(dR_{[0]}/dt)$ and $(dy_{[0]}/dt)/(dR_{[0]}/dt)$ are substituted into (A 15) to yield $dR_{[0]}/dt$. This completes the solution, and again $dR_{[0]}/dt$ and $d\Gamma_{[0]}/dt$ vary with time implicity through $R_{[0]}$ (or equivalently $V_{[0]}$).

We thank the National Science Foundation (PYI grant no. CTS-8658147 to D. R.), the ACS Petroleum Research Fund (no. 27403-AC9 to D. R. and no. 29378-AC9 to C. M.), and Mechanical Engineering Department at Louisiana State University (start-up fund for H. W.) for supporting this work.

REFERENCES

Agrawal, M. L. & Neuman, R. D. 1988 Surface diffusion in monomolecular films II. Experiment and theory. *J. Colloid Interface Sci.* **121**, 366–380.

Aveyard, R. & Haydon, D. A. 1973 An *Introduction to the Principles of Surface Chemistry*. Cambridge University Press.

Baret, J. F. 1969 Theoretical model for an interface allowing a kinetic study of adsorption. *J. Colloid and Interface Sci.* **30**, 1–12.

Borwankar, R. P. & Wasan, D. T. 1983 The kinetics of adsorption of surface active agents at gas–liquid surfaces. *Chem. Engng Sci.* **38**, 1637–1649.

Chang, C. & Franses, E. 1994*a* An analysis of the factors affecting dynamic tension measurements with the pulsating bubble surfactometer. *J. Colloid Interface Sci.* **164**, 107–113.

Chang, C. & Franses, E. 1994*b* Dynamic surface tension behavior of aqueous octanol solutions under constant area and pulsating area conditions. *Chem. Engng Sci.* **49**, 313–325.

Chang, C.-H. & Franses, E. 1995 Adsorption dynamics of surfactants at the air/water interface: A critical review of mathematical models, data and mechanisms. *Colloids Surfaces* A **100**, 1–45.

Faour, G., Grimaldi, M., Richou, J. & Bois, A. 1996 Real-time pendant drop tensiometer using image processing with interfacial area and interfacial tension control capabilities. *J. Colloid Interface Sci.* **181**, 385–392.

Gaines, G. L., Jr. 1966 *Insoluble Monolayers at Liquid–Gas Interfaces*. Interscience, New York.

Hallowell, C. & Hirt, D. E. 1994 Unusual characteristics of the maximum bubble pressure method using a Teflon capillary. *J. Colloid Interface Sci.* **168**, 281–288.

Hirt, D. E., Prud'homme, R. K., Miller, B. & Rebenfield, L. 1990 Dynamic surface tensions of hydrocarbon and fluorocarbon surfactant solutions using the maximum bubble pressure method. *Colloids Surfaces* **44**, 101.

Joos, P. & Uffelen, M. V. 1995 Adsorption kinetics with surface dilatation. I. Desorption of slightly soluble monolayers at constant surface pressure. *J. Colloid Interface Sci.* **155**, 271–282.

Liggieri, L., Ravera, F. & Passerone, A. 1995 Dynamic interfacial tension measurements by a capillary pressure method. *J. Colloid Interface Sci.* **169**, 226–237.

Lin, S. Y., McKeigue, K. & Maldarelli, C. 1990 Diffusion controlled pendant drop digitization. *AIChE J.* **36**, 1785–1795.

Macleod, C. A. & Radke, C. J. 1993 A growing drop technique for measuring dynamic interfacial tension. *J. Colloid Interface Sci.* **160**, 435–448.

Macleod, C. A. & Radke, C. J. 1994 Surfactant exchange kinetics at the air/water interface from the dynamic tension of growing drops. *J. Colloid Interface Sci.* **166**, 73–93.

Miller, R., Joos, P. & Fainerman, V. B. 1994 Dynamic surface and interfacial tensions of surfactant and polymer solutions. *Adv. Colloid Interface Sci.* **49**, 249–302.

Milliken, W. J. & Leal, L. G. 1994 The influence of surfactant on the deformation and breakup of a viscous drop: The effect of surfactant solubility. *J. Colloid Interface Sci.* **166**, 275–285.

Milliken, W. J., Stone, H. A. & Leal, L. G. 1993 The effect of surfactant on the transient motion of Newtonian drops. *Phys. Fluids* A **5**, 69–79.

Nagarajan, R. & Wasan, D. T. 1993 Measurement of dynamic interfacial tension by an expanding drop tensiometer. *J. Colloid Interface Sci.* **159**, 164–175.

Passerone, A., Liggieri, L., Rando, N., Ravera, F. & Ricci, E. 1991 A new experimental method for the measurement of interfacial tension between immiscible fluids at zero bond number. *J. Colloid Interface Sci.* **146**, 152.

Pozrikidis, C. 1992 *Boundary Integral and Singularity Methods for Linearized Viscous Flow*. Cambridge University Press.

Rio, O. I. der & Neumann, A. W. 1997 Axisymmetric drop shape analysis: computational methods for the measurement of interfacial properties from the shape and dimensions of pendant and sessile drops. *J. Colloid Interface Sci.* **196**, 136–147.

Sadhal, S. S. & Johnson, R. E. 1983 Stokes flow past bubbles and drops partially coated with thin films. Part I. Stagnant cap of surfactant film-exact solution. *J. Fluid Mech.* **126**, 237–250.

Scriven, L. E. 1960 Dynamics of a fluid interface. *Chem. Engng Sci.* **12**, 98–108.

Slattery, J. C. 1990 *Interfacial Transport Phenomena*. Springer, New York.

Song, B. & Springer, J. 1996 Determination of interfacial tension from the profile of a pendant drop using computer-aided image processing. 1. Theoretical. *J. Colloid Interface Sci.* **184**, 64–76.

Stone, H. A. & Leal, L. G. 1990 The effects of surfactants on drop deformation and breakup. *J. Fluid Mech.* **220**, 161–186.

Waxman, A. M. 1984 Dynamics of a couple-stress fluid membrane. *Stud. Appl. Maths* **70**, 63–86.

Wong, H., Rumschitzki, D. & Maldarelli, C. 1996 On the surfactant mass balance at a deforming fluid interface. *Phys. Fluids* **8**, 3203–3204.

Wong, H., Rumschitzki, D. & Maldarelli, C. 1998 Theory and experiment on the low-Reynolds-number expansion and contraction of a bubble pinned at a submerged tube tip. *J. Fluid Mech.* **356**, 93–124.

Zhang, X., Harris, M. & Basaran, O. 1994 Measurement of dynamic surface tension by the growing drop technique. *J. Colloid Interface Sci.* **168**, 47–60.